# INTERNATIONAL SOCIETY FOR SOIL MECHANICS AND GEOTECHNICAL ENGINEERING



This paper was downloaded from the Online Library of the International Society for Soil Mechanics and Geotechnical Engineering (ISSMGE). The library is available here:

https://www.issmge.org/publications/online-library

This is an open-access database that archives thousands of papers published under the Auspices of the ISSMGE and maintained by the Innovation and Development Committee of ISSMGE.

# Liquefaction evaluation directly comparing upward wave energy with dissipated energy



Takaji Kokusho (Professor Emeritus) Chuo University, Tokyo, Japan

#### **ABSTRACT**

The author already proposed an energy-based liquefaction evaluation method (EBM), wherein upward wave energy as the energy demand is directly compared with the energy capacity or dissipated energy in soil deposits. The proposed EBM are characterized here in terms of how to evaluate the energy demand by upward earthquake waves, how closely the dissipated energy determines residual strains for different earthquake motions, and how to compare the demand and capacity simply and reasonably. The EBM procedures and evaluation examples are also described in comparison with the conventional Stress-Based Method (SBM). The comparative studies have demonstrated that, for a normal ground motion, EBM tends to give basically similar results to SBM. However, disparities appear between them for ground motions with small peak accelerations and high energy or high accelerations and low energy. Considering that the dissipated energy controls liquefaction mechanism as lab tests indicate, it is recommended to employ the EBM to supplement SBM for various earthquake motions, wherein engineers can grasp the energy demand of design motion at a glance.

#### 1. INTRODUCTION

Since 1970's, the stress-based method (SBM) has been exclusively used in liquefaction potential evaluations in current engineering practice. In SBM, the CRR (Cyclic resistance ratio) is compared with CSR (Cyclic Stress Ratio) during design earthquakes, wherein the key issue is how irregular seismic motions are properly represented by harmonic motions with equivalent amplitudes and numbers of cycles considering pertinent wave parameters. An energy-based method (EBM) also proposed for liquefaction evaluation a few decades ago has not yet been employed in practice. Unlike the stress-based method (SBM), EBM can directly deal with irregular seismic motions without being converted to harmonic motions. Namely, the liquefaction energy capacity can simply be compared with the wave energy demand of earthquake motions without any additional considerations necessary.

The EBM was first proposed by Davis and Berrill (1982), following a theoretical paper by Nemat-Nasser and Shokooh (1979) that the pore-pressure buildup is directly related to the amount of energy dissipated in the unit volume of soil (dissipated energy density). In their method, the dissipated energy in liquefiable sand (capacity) was directly correlated with seismic energy (demand). The energy arriving at a site was calculated by empirical formulas, though it was not explained at which depth the incident energy is given, or how it transmits upward to liquefiable sand layers. Instead, variables consisting of earthquake magnitude, source distance and other pertinent parameters were calculated in liquefied/non-liquefied sites individually during previous earthquakes. They were directly plotted versus corrected SPT N-values in a chart and compared with liquefaction case histories to empirically obtain a boundary curve discriminating liquefaction/non-liquefaction.

Kazama et al. (1999) proposed an energy-based scheme to evaluate liquefaction potential, in which cumulative dissipated energy in soil layers due to a given seismic motion was evaluated in one-dimensional equivalent

linear analysis and compared with the energy capacity for the soil layers to liquefy.

As for experimental research on the energy capacity for liquefaction, undrained cyclic loading tests focusing on the dissipated energy in soil specimens were conducted using a torsional simple shear apparatus by Towhata and Ishihara (1985), in which a unique relationship was found between shear work (dissipated energy) and excess porepressure being independent of the shear stress history. Yanagisawa and Sugano (1994) conducted similar cyclic shear tests on the effect of irregularity of cyclic stress on the dissipated energy to find a unique relationship. Laboratory soil tests were also conducted by Figueroa et al. (1994) using a strain-controlled torsional shear device, which demonstrated that the dissipated energy per unit volume during cyclic loading was closely connected to pore-pressure buildup under different confining stresses.

Kokusho (2013) proposed EBM to evaluate in situ liquefaction potential by directly evaluating upward seismic wave energy  $E_u$  (the energy demand) and comparing it with the energy capacity of a liquefiable layer. To the best of the present author's knowledge, there has been no engineering attempt to directly utilize the seismic wave energy as energy demand for design. It actually has a great advantage that even for the two extreme earthquake motions, for example with the long duration 2011 Tohoku earthquake of three minutes and the short duration 1995 Kobe earthquake of only 20 seconds, the energy demand can be grasped at a glance with almost no attention to durations, dominant periods and wave forms. For liquefaction problems in soil deposits and soil structures where residual strains and failures are determined in terms of the dissipated energy or energy capacity, the EBM comparing the energy demand with the energy capacity is promising.

It may be necessary here to point out with respect to the dimension of energy to be used in the following that the wave energy is in kJ/m² (energy per unit area) while the strain/dissipated energy by cyclic loading soil tests is in kJ/m³ (energy per unit volume=energy density), though

both are written simply as "energy" for simplicity except when it is necessary to distinguish.

In the following, the present EBM are characterized in terms of how to evaluate the energy demand by upward earthquake waves, how closely the energy capacity determines residual strains for different seismic motions, and how to compare the demand and capacity reasonably. Finally the EBM procedures and some examples are described in comparison with SBM.

#### 2. HOW TO EVALUATE ENERGY DEMAND

Let us consider the wave energy in the upward SH-wave with the wave velocity  $V_{\rm S}$  passing through a horizontal plane A-A' of a unit area as illustrated in Figure. 1. Kinetic energy in a soil element of a unit horizontal area times a small thickness  $dz = V_{\rm S} \Delta t$  (a travel distance in a short time increment  $\Delta t$ ) having particle velocity  $\dot{u}$  can be expressed as:

$$\Delta E_k = \frac{1}{2} \rho V_s \Delta t \left( \dot{u} \right)^2$$
 [1]

Strain energy simultaneously induced by the wave propagation in the same thin soil element is expressed by shear stress  $\tau = G\gamma$ , shear strain  $\gamma$ , and using  $\gamma = -\dot{u}/V_s$  as:

$$\Delta E_{e} = \int_{0}^{\gamma} (V_{s} \Delta t) \tau d\gamma = \frac{1}{2} \rho V_{s} \Delta t (\dot{u})^{2}$$
 [2]

Hence,  $\Delta E_k = \Delta E_e$ , and the wave energy passing through the unit area in the time increment  $\Delta t$  is their sum expressed as:

$$\Delta E = \Delta E_k + \Delta E_e = \rho V_s \Delta t \left( \dot{u} \right)^2$$
 [3]

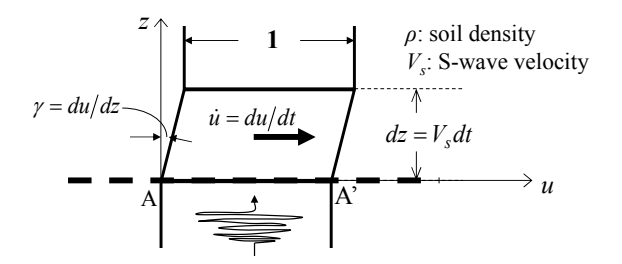


Figure. 1: Schematic illustration on wave energy in upward SH-wave propagation

Hence, the cumulative energy in a time interval  $t=t_1\sim t_2$  can be expressed as the sum of the kinetic and strain energies,  $E_k$  and  $E_e$ , of the equal amount (Timoshenko and Goodier 1951, Sarma 1971) as:

$$E = E_k + E_e = \rho V_s \int_{t_1}^{t_2} (\dot{u})^2 dt$$
 [4]

Eq. 4 clearly tells us the basic fact that wave amplitudes alone, either accelerations or velocities, are meaningless without associated impedance  $\rho V_{\rm s}$  in determining seismic damage in terms of energy.

Thus, the wave energy is defined for the onedirectionally propagating wave. In order to calculate the energy flow from earthquake records at or below the ground surface assuming the one-dimensional vertical propagation of SH-waves, it is necessary to separate a recorded motion into upward and downward waves. In the multiple reflection theory of the SH wave, a level ground is idealized by a set of horizontal soil layers as shown in Figure. 2. Let  $E_{u,m}$ ,  $E_{d,m}$  denote the upward and downward energies at the upper boundary of the  $m^{th}$ layer and  $\boldsymbol{E}_{u,m-1}$  ,  $\boldsymbol{E}_{d,m-1}$  the corresponding energies at the upper boundary of the  $(m-1)^{th}$  layer, respectively. Because of the internal damping, the upward and downward energies at the lower boundary of the (m-1)th layer may be different from  $E_{u,m-1}$ ,  $E_{d,m-1}$  and denoted here as  $E_{u,m-1}'$ ,  $E_{d,m-1}'$ . Then, it is easy to understand that the principle of energy conservation holds at the boundary between mth and (m-1)th layer as:

$$E_{u,m} + E'_{d,m-1} = E'_{u,m-1} + E_{d,m} \equiv E_t$$
 [5]

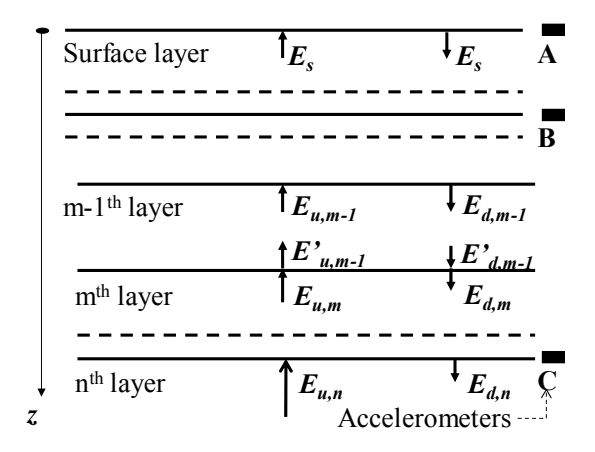


Figure 2. Level ground idealized by a set of horizontal soil layers with vertical array seismometers A, B. C.

If the wave energies are evaluated at the end of a given earthquake shaking, the energy  $E_t$  in Eq. 5 means the gross energy passing through the boundary during the earthquake. From Eq. 5, the next equation is derived.

$$E_{u,m} - E_{d,m} = E'_{u,m-1} - E'_{d,m-1} \equiv E_w$$
 [6]

Here,  $E_w$  stands for the energy dissipated in soil layers above the layer boundary during the earthquake, because all the energy computed here is assumed to transmit vertically in this evaluation. It is also clear that the dissipated energy  $E_w$  can be calculated from  $E_u$  and  $E_d$  not only at the layer boundary but also at any intermediate depth as:

$$E_w = E_u - E_d \tag{7}$$

Based on the multiple reflection theory, upward and downward SH waves and hence corresponding wave energies at arbitrary levels can be evaluated from a single record at any level using the free surface boundary condition (Schnabel et al. 1972). If vertical array records are available, however, they will considerably improve the energy flow evaluation which may not fully comply with the simple theory. Suppose that the seismic records are obtained not only at the ground surface (Point A) but also at two subsurface levels, B and C as illustrated in Figure 2. Then, the energy flow between B and C can be calculated by using earthquake records at the two levels (Kokusho and Motoyama, 2002) where seismic wave is less

contaminated by strong soil nonlinearity manifested near the surface. For the energy evaluation between the ground surface (Point A) and downhole (Point B), two sets of energy flow can be calculated using the earthquake record either at A or B combined with the boundary condition at the free surface. The two sets are then averaged with the weight of relative proximity to the corresponding points to have the averaged energy flow.

Typical examples of calculated energy flow are shown in two sites; (1) Port Island (PI) and (2) Taiki (TKCH08: KiKnet) in Hokkaido.

#### 2.1 Port Island (PI) site

All soils are Quaternary to the deepest depth, and  $V_{\rm S}$  at the deepest level is lower than 400 m/s. Extensive lique-faction occurred in surface reclaimed soil (water table at GL.-4.0 m) down to 17.5 m from the surface, which lowered  $V_{\rm S}$  there. Main shock records in two horizontal directions at 3 levels (Point A: GL.-0 m, B: -32.4 m and C: -83.4 m) were used for the energy evaluation.

In the lower two panels of Figure 3(a), particle velocity time histories at the surface (GL.0 m) are shown in two orthogonal horizontal directions (the maximum acceleration direction and perpendicular to that direction). In the top panel, the energy at the surface  $E_s$  as a sum of the two directions (calculated from the velocity time histories and the impedance of the surface layer) is shown. In the lower two panels of Figure 3(b), upward and downward velocity waves at the deepest level (GL.-83.4 m) are shown in the two directions. In the top, the time histories of the energies at the deepest level calculated from the velocities are shown. Note that the upward and downward energies,  $E_u$  and  $E_d$ , show time-dependent monotonic increase because they are the cumulative energy

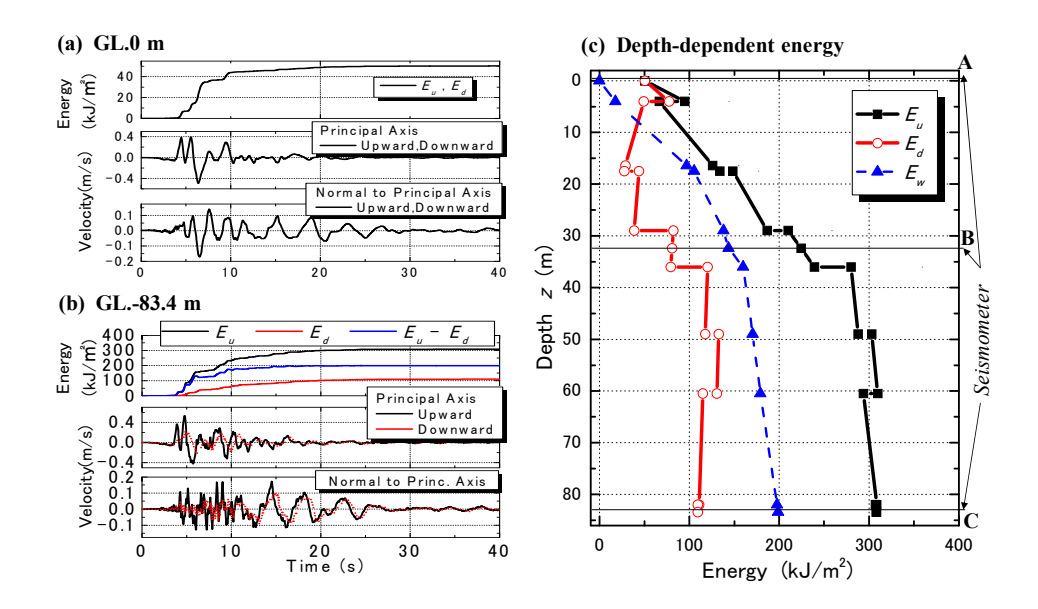


Figure 3: Calculation of wave energies in PI: (a) Time-histories of energy and velocity at GL.0m, (b) the same at GL.-83.4 m, (c) Depth-dependent energy distributions. (Kokusho and Suzuki 2011)

transmitted by one-directionally propagating waves. In contrast, the difference  $(E_u - E_d)$  indicates the energy balance in soil layers upper than a given level and hence shows both increase and decrease with time.

Figure 3(c) shows the distributions of the energies,  $E_u$ ,  $E_d$ ,  $E_w$  along the depth summed up in the two directions. The energies between B and C are uniquely determined from the combination of seismic Records B and C based on the multi-reflection theory (Kokusho and Motoyama 2002). In contrast, either Record A at the surface or B is sufficient to calculate the distribution between A and B, where the free surface condition is available. In the PI site, where strong soil nonlinearity due to extensive liquefaction occurred in surface layers, Record B was exclusively used, for the calculation between A and B because it was likely to be less influenced by soil nonlinearity than Record A. Record A was used only for computing the energy at the surface A, which was 50 kJ/m² in contrast to 86 kJ/m² calculated from Record B.

The energies at Point B obtained from the combination of Record B and C were  $E_u$  =236 kJ/m² and  $E_d$  =80 kJ/m² whereas those from Record B together with the free surface condition were  $E_u$  =212 kJ/m² and  $E_d$  =82 kJ/m². Though the differences were not large, the energies  $E_u$  and  $E_d$  at the accelerometers of intermediate depths were averaged. In order to avoid anomalous depth-dependent variation near the intermediate accelerometers in the energies  $E_w$  calculated by Eq.6 due to the averaging procedure, the following modifications were implemented.

$$E_w = (E_{u,m} - E_{d,m})/2 + (E'_{u,m-1} - E'_{d,m-1})/2$$
 [8]

Figure 3(c) shows obvious decreasing trend of  $E_d$  from the deepest level to the surface with decreasing depth particularly in the top 36 m. The downward energy  $E_d$  is evidently smaller in the top 36 m than the deeper part.

The dissipated energy  $E_{\rm w}$  tends to monotonically increase with increasing depth. The increasing rate from the surface down to 17.5 m deep, where extensive lique-faction occurred in reclaimed soil, is particularly large, indicating that the energy loss per unit volume in liquefied sandy soil was 6 kJ/m³ on average. This value seems to be comparable with dissipated energy density  $\Delta W$  measured in laboratory tests as will be seen in Figure 7(b).

#### 2.2 Taiki (TKCH08: KiK-net) site

Quite different from the PI site, the rock at the deepest point (GL.-100 m) is very stiff (Vs=2800 m/s) here, while small-strain  $V_s$  in the surface layer is as low as  $V_s$ =130 m, which further degraded during the main shock. Main shock records in two horizontal directions at the surface (Point A) and the deepest level at GL.-100 m (Point B) were used for the energy flow evaluation.

In the lower two panels of Figure 4(a), particle velocity time histories at the surface (GL.0 m), calculated from Record A are shown in NS and EW directions. In the top panel, the incident energy at the surface calculated from the velocity time histories and the impedance at A are shown as the sum in the two directions. In Figure 4(b), velocity time histories of upward and downward waves at the deepest level of GL.-100 m calculated from Record B

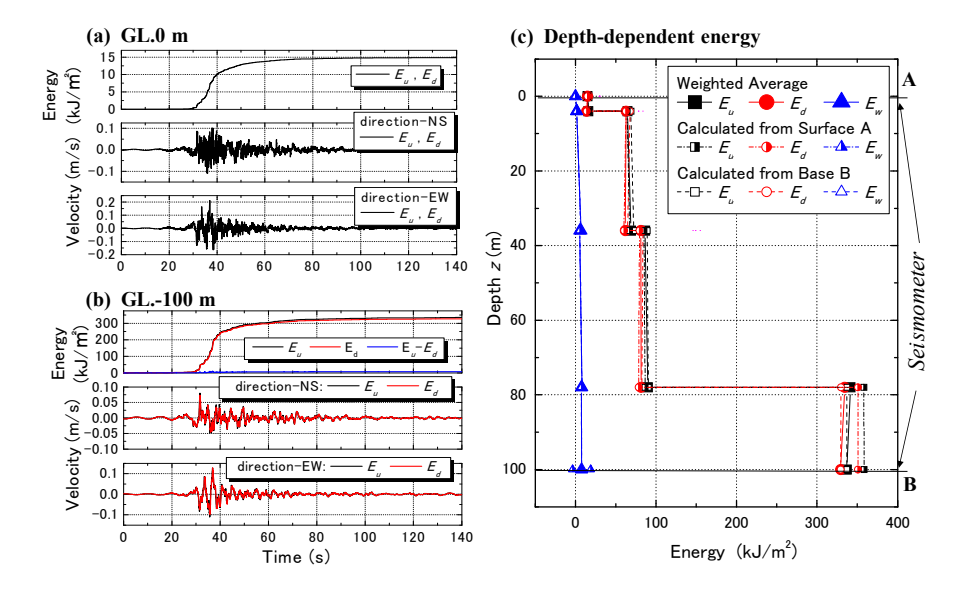


Figure 4. Calculation of wave energies in KiK-NET Taiki: (a) Time-histories of energy and velocity at GL.0m. (b) the same at GL.-100 m, (c) Depth-dependent energy distributions (Kokusho and Suzuki 2011).

in the two directions and the energy time histories at the same level are shown in the same manner. Both upward and downward energies,  $E_u$  and  $E_d$ , show rapid increase with a marginal difference to each other, resulting in a small value of  $\left(E_u-E_d\right)$ , indicating that energy dissipation in this site is very small, reflecting the very stiff soil condition in the deeper portion.

In Figure 4(c), energy flows along depth are calculated either from Record A at the surface or from Record B at the base combined with the free surface condition, and plotted with open symbols with chain-dotted and dashed lines, respectively. The solid thick lines with close symbols are the average of the two calculations with the weight of the proximity to the levels B and A. The two energy flows calculated from Record A and B are very similar to each other to make it difficult to distinguish the above mentioned three lines, indicating the soil model is a good reproduction of the actual ground at this particular site, which was not always the case. Thus, the averaging procedure tends to modify the depth-dependent energy variations to a certain degree, though the energy values at the base and at the surface is unaffected by this procedure and hence the global trend in energy flow, too.

In Taiki-site, despite almost the same upward energy, more than 300 kJ/m², as in PI at the deepest level, less than 100 kJ/m² passed through the boundary (GL.-78 m) with a drastic impedance change and only 15 kJ/m² reached the soil surface eventually. A small difference between  $E_u$  and  $E_d$  indicates that the considerable upward energy was reflected at the boundaries and returned to the deeper ground, before arriving to the soft soil layer near the surface. This also means that the dissipated energy  $E_w$  could not be large because the most energy transmitted only in stiff layers wherein the energy loss is small.

#### 2.3 General trends of upward energy

Figure 5 depicts the variations of upward energy  $E_u$  along the depth z calculated for 9 earthquakes at 30 vertical array sites. On account of large differences in the energies depending on sites and depths, the horizontal axis is taken as logarithmic. Like the two sites, PI and Taiki explained above, the upward energy shows obvious decreasing trend in most sites with decreasing depth irrespective of the differences in the absolute value of the upward energy. In some sites, the  $E_u$ -value decreases to less than 1/10 from the base to the surface. The decreasing trend is more pronounced in the shallow part, particularly near the surface, and less conspicuous below the depth of 50 m - 100 m.

Out of the depth-dependent upward energy variations at 30 sites in Figure 5, 24 sites have been used further for the following energy analyses. These sites have been chosen because the difference in upward energies at the deepest level calculated from measured motions at the ground surface and the deepest level (Kokusho and Suzuki 2011) were within about 25%. The upward energy ratio and the impedance ratio:

$$\beta = (E_u)_i / (E_u)_{i+1}$$
 [9]

$$\alpha = (\rho V_s)_i / (\rho V_s)_{i+1}$$
 [10]

are calculated, respectively, between two neighboring layers, i and i+1, for i=1 to n-1 from the surface to the base layer of vertical array sites as indicated in Figure 2. Here,  $E_u$  = the upward energy at the upper boundary,  $\rho$  =soil density and  $V_s$ =S-wave velocity optimized for main

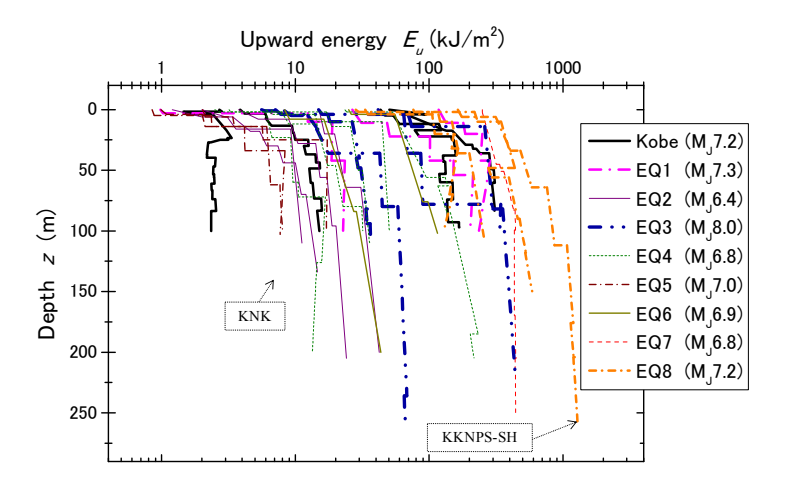


Figure 5. Variations of upward energy  $E_u$  along depth calculated for 9 earthquakes at 30 vertical array sites (Kokusho and Suzuki 2011).

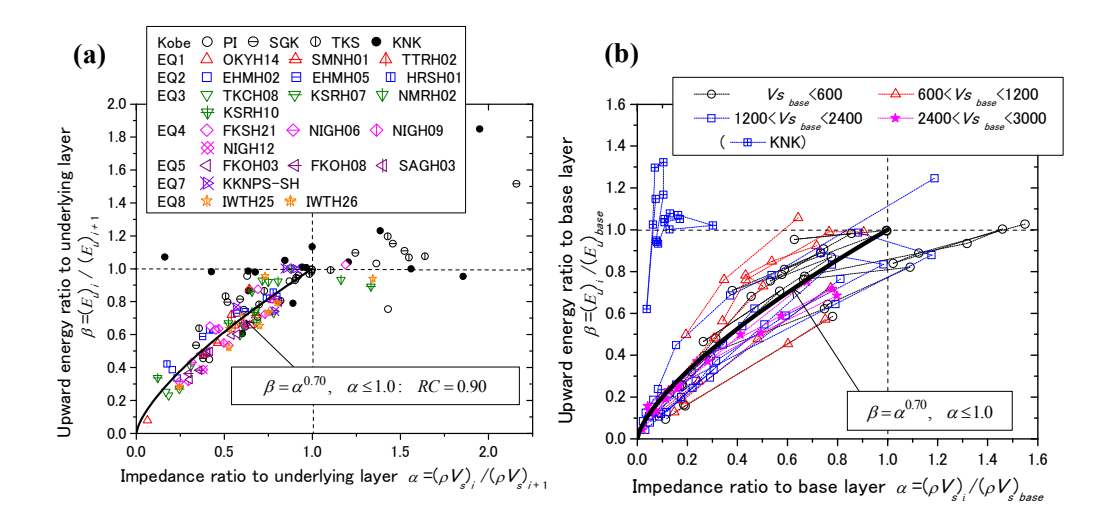


Figure 6. Impedance ratios  $\alpha$  versus corresponding upward energy ratios compared with empirical formula: (a) between neighboring layers, (b) between given layer and base layer. (Kokusho and Suzuki 2012)

shock motions in each layer. The soil density  $\rho$  is determined as 1.6 $\sim$ 2.0 t/m³ for  $V_s$ ≤300 m/s, 2.0 $\sim$ 2.2 t/m³ for 300 m/s ≤ $V_s$ ≤700 m/s, 2.3 $\sim$ 2.4 t/m³ for 700 m/s ≤ $V_s$ ≤1000 m/s, 2.5 $\sim$ 2.7 t/m³ for 1000 m/s ≤ $V_s$ <3000 m/s.

In Figure 6(a), the energy ratios  $\beta$  are plotted versus the corresponding impedance ratios  $\alpha$  for all the layers above the deepest levels in the 24 vertical array sites with different symbols. For the majority of the data points,  $\alpha \le 1.0$  because the impedance ratio is normally less than unity. In this region of the  $\alpha$ -value, it is quite reasonable to assume that  $\beta$ =0 for  $\alpha$ =0, and  $\beta$ =1 for  $\alpha$ =1 (uniform layer). Hence, a simple power function  $\beta=\alpha^n$  may be used to approximate the plots and the power n=0.70 can be obtained from the least mean-square method with the regression coefficient RC=0.90.

$$\beta = \alpha^{0.70}$$
,  $\alpha \le 1.0$  [11]

In this statistical computation, the data points of KNK site, shown with a solid circle in Figure 6(a), are omitted because they are evidently biased from others probably due to some site-specific problems. Thus, Eq. 11 shown in Figure 6(a) with a thick solid curve, approximates the data points fairly well up to  $\alpha=1.0$ , if the energy ratio and the impedance ratio of two neighboring layers are concerned, despite that soil conditions included here are very variable from stiff rock almost equivalent to seismological bedrock in the great depth to soft soil near ground surface.

The problem is how far the same fitting by Eq. 11 can be applicable to layers not necessarily neighboring but separating from each other. In order to examine this, the upward energy ratio  $\beta$  and the impedance ratio  $\alpha$  are

redefined here between a layer i (i =1 to n-1 as shown in Figure 2) and the deepest layer (base layer) as:

$$\beta = \left(E_{u}\right)_{i} / \left(E_{u}\right)_{base}$$
 [12]

$$\alpha = (\rho V_s)_i / (\rho V_s)_{\text{base}}$$
 [13]

where  $(E_u)_{base}$  and  $(\rho V_s)_{base}$  are the upward energy and the seismic impedance of the base layer, respectively. In Figure 6(b), data points for all layers at the 24 vertical array sites are plotted on the  $\alpha$  -  $\beta$  diagram. In this chart, symbols are connected with dashed lines for individual sites and differentiated according to 4 classes of Vsvalues at the base layer. Due to averaging operations of energies calculated from the base and surface motions as mentioned before and also due to the reverse layers in terms of the impedance, the plots here are more dispersed than those in Figure 6(a). Nevertheless, the curve by Eq. 11 using  $\alpha$  and  $\beta$  redefined in Eqs. 12 and 13 and superposed here again, seems to represent the plots on average. Among the plots, the star symbols for the sites where the impedances of the deepest base layer are almost equivalent to seismological bedrock (2400 m/s < Vs < 3000 m/s) fit well with the curve near the origin (at smaller  $\alpha$  -values corresponding to the ground surface) in particular. This indicates that it may be possible to use Eq. 11 to evaluate the upward energy in a soil layer near the ground surface from the upward energy at a base almost as stiff as the seismological bedrock by considering the impedance ratio between the two corresponding layers.

#### 2.4 Upward energy at a given layer

Based on Eq.11 it may be possible to determine the upward energy in a given layer where liquefaction potential is to be evaluated. Kokusho and Suzuki (2011) quantified the incident wave energies  $E_{IP}$  at the deepest levels of a number of vertical array sites using nine strong earthquakes. It was found that, despite considerable data dispersions, the  $E_{IP}$ -values plotted versus hypocenter distances R are basically in accordance with the well-known empirical formulas.

$$E_{IP} = E_{Total} / (4\pi R^2)$$
 [14]

$$\log E_{Total} = 1.5M + 1.8$$
 [15]

Here,  $E_{IP}$  is in kJ/m², R in meter, and  $E_{Total}$  is the total wave energy released during individual earthquakes in kJ originally from Gutenberg (1956). Because the impedance  $\rho V_s$  at the base of vertical arrays are very variable, the  $E_{IP}$ -values at the seismological bedrocks, using their  $V_s$ =3000 m/s and  $\rho$ =2.7 t/m³, were further calculated using Eq. 11 again, assuming the vertical propagation of SH-wave still applicable in the great depth (Kokusho and Suzuki 2012). Despite considerable data scatters pre sumable due to various fault mechanisms, the values at the seismological bedrock seems to fit better with Eqs. 14 ,15. Thus, combining Eqs.14, 15 with Eq.11, the upward energy at a given soil layer may be roughly determined for liquefaction evaluations.

On the other hand, if design acceleration motions are

given at ground surface as in many engineering projects, the upward energy can be readily calculated in Eq.4 by conducting one-dimensional response analyses if the properties of soil profile are available. In the later section of this paper, the site-specific energies are calculated from ground surface acceleration records in order to compare with the SBM liquefaction evaluation.

### 3. DISSIPATED ENERGY VERSUS LIQUEFACTION BEHAVIOR FOR DIFFERENT MOTIONS

#### 3.1 Test results by harmonic motion

Figure 7(a) typically shows how the dissipated energy  $\Delta W$  in a single loading cycle is defined as the internal area of the stress-strain hysteresis loop A-B-C-D in cyclic triaxial tests. The triangular area OBB' means the maximum elastic strain energy in the cyclic loading and denoted as W. Accumulated dissipated energy per unit volume is obtained by adding  $\Delta W$  in each cycle of loading to a k-th cycle as,

$$\sum \Delta W = \sum_{k} \left( \int_{A}^{D} \sigma_{d} d\varepsilon \right)_{k}$$
 [16]

In Figure 7(b), the excess pore-pressure normalized by the initial effective stress  $\Delta u/\sigma_c$ ' and strain amplitude  $\varepsilon_{DA}$  in the vertical axes are plotted against the cumulative dissipated energy  $\sum \Delta W/\sigma_c$ ' in the horizontal axis with different symbols for  $D_r\approx 30$ , 50 and 70%. Here, the dissipated energy per unit volume  $\Delta W$  is normalized by the effective confining stress  $\sigma_c$ ', where  $\Delta W$  has the dimension of stress. This normalization is meaningful also because the cumulative dissipated energy  $\Sigma \Delta W$  for pore-pressure

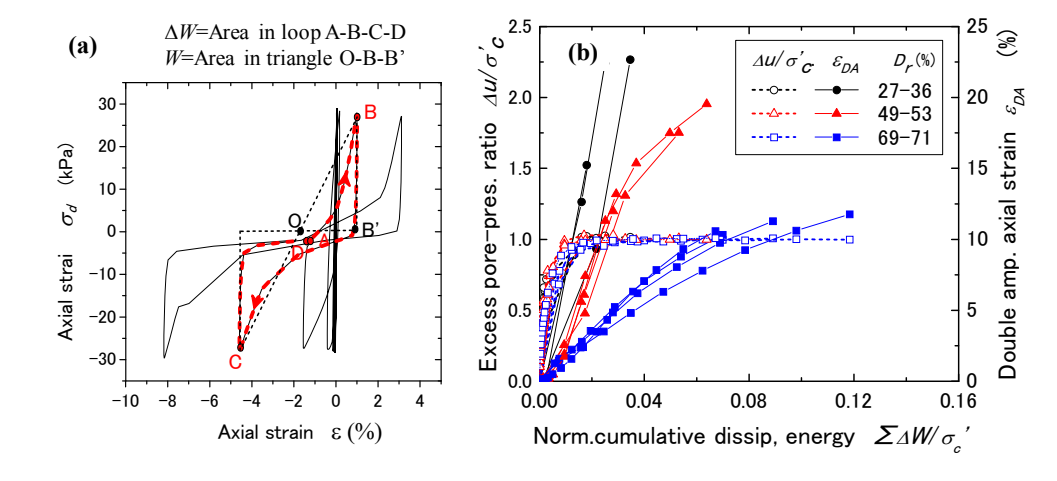


Figure 7. Cyclic triaxial liquefaction test results: (a) Dissipated and maximum elastic energies,  $\Delta W$  and W, in typical stress-strain curves, (b) Normalized cumulative dissipated energy versus excess pore-pressure ratio or double amplitude axial strain obtained from a series of Cyclic triaxial tests (Kokusho 2013).

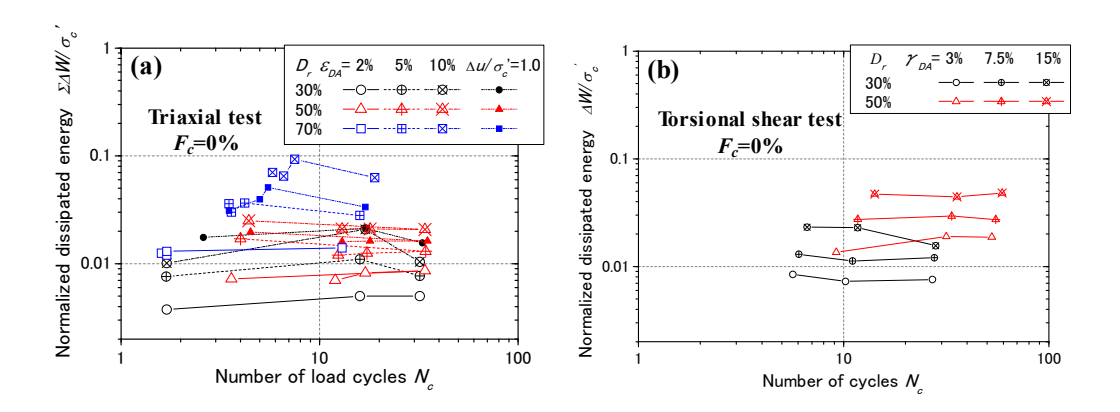


Figure 8. Normalized cumulative dissipated energy for given strains or pore-pressure buildup versus number of cycles: (a) Cyclic triaxial test (Kokusho et al. 2013), (b) Torsional shear test (Kaneko 2015).

buildup or given induced strain was found to increase almost in proportion to the confining stress (Figueroa et al. 1990, Kaneko 2015). In Figure 7(b), the pore-pressure buildup correlates well with the dissipated energy, and becomes  $\Delta u/\sigma_c$ '=1.0 at around  $\sum \Delta W/\sigma_c$ '=0.02. It is remarkable that the difference in the  $\Delta u/\sigma_c$ '- $\sum \Delta W/\sigma_c$ ' correlation for different  $D_r$  is small, while the  $\varepsilon_{DA}$  ~ $\sum \Delta W/\sigma_c$ ' correlation is dependent on  $D_r$ . For individual  $D_r$ -values, the cumulative dissipated energy  $\sum \Delta W/\sigma_c$ ' can be correlated consistently with the strain  $\varepsilon_{DA}$  not only up to the initial liquefaction ( $\varepsilon_{DA}$ =5%) but also even after that, almost and serves as an indicator for the severity of liquefaction.

In Figure 8(a), the dissipated energies  $\sum \Delta W/\sigma_c$  are plotted in the vertical axis of log-log charts versus the number of cycles  $N_c$  in the horizontal axis to attain specific values of strain amplitudes,  $\varepsilon_{DA}$ =2, 5, 10%, or pressure buildup,  $\Delta u/\sigma_c$ '=1.0 in triaxial tests on clean sands. There are groups of 2 to 4 data-points with identical symbols in the charts corresponding to the same specific strains  $\varepsilon_{DA}$ or  $\Delta u/\sigma_c$ '=1.0 having different number of loading cycles  $N_c$ . The lines connecting the same symbols do not show consistent increasing or decreasing trend of  $\sum \Delta W/\sigma_c$ 'values with increasing  $N_c$ , despite those for dense sands showing non-systematic up-down trends particularly in higher strains. Figure 8(b) shows similar plots obtained by torsional simple shear tests using the same clean sand. The plots are for attaining specific values of strain amplitudes,  $\gamma_{DA}$ =3, 7.5, 15%. From the two diagrams, the lines connecting the same symbols may be judged to be essentially flat for easily liquefiable loose sands with lower  $\sum \Delta W/\sigma_c$ '-values. Dense sands of  $D_c$ =70%, tend to show up-down variations of the energy against Nc, presumably reflecting the cyclic mobility response. This observation seems to indicate that the dissipated energy  $\sum \Delta W/\sigma_c$ almost uniquely determines the strain amplitude or porepressure buildup for loose sands irrespective of  $N_c$  and CSR to attain a particular strain amplitude or pressure buildup. This further indicates that a CSR-N<sub>c</sub> line corresponding to particular strain or pore-pressure buildup, which is normally considered as a basis for the SBM liguefaction evaluation, also represents the lines of equal

dissipated energy. This observation paves a way to EBM using soil test data in SBM.

From the  $CSR\sim N_c$  chart in Figure 8 obtained by cyclic loading tests, CRR for  $N_c$ =20 for example can be determined for  $\varepsilon_{DA}$ =2, 5, 10%, and  $\Delta u/\sigma_c$ '=1.0. The CRR-values are directly correlated with corresponding dissipated energy  $\sum \Delta W/\sigma_c$ ' calculated from the same test data to develop a  $CRR\sim\sum\Delta W/\sigma_c$ ' chart shown in Figure 9 (Kokusho 2013). Note that the values  $\sum\Delta W/\sigma_c$ ' in the vertical axis correspond to the dissipated energies needed to attain the axial strain  $\varepsilon_{DA}$ =5% by arbitrary stress amplitudes and corresponding numbers of cycles, while the CRR-values in the horizontal axis represent the stress amplitudes at  $N_c$ =20. Despite some data scatters, the CRR-value for the strain level  $\varepsilon_{DA}$ =5% (open circles) seems to be uniquely correlated with  $\sum\Delta W/\sigma_c$ ' for sands with differ-

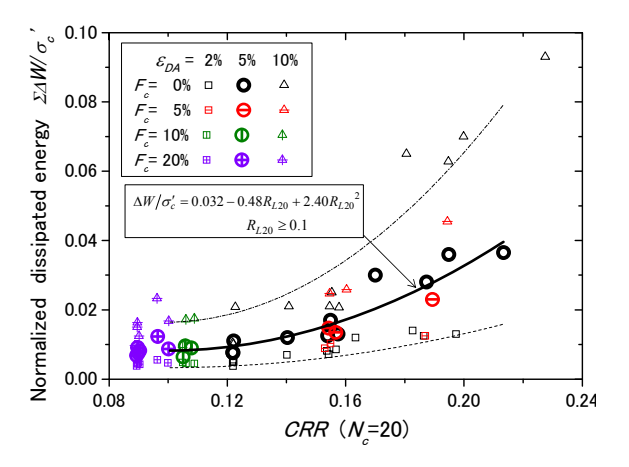


Figure 9: CRR ( $N_c$ =20) versus  $\sum \Delta W/\sigma_c$ ' plots for various  $D_r$  and  $F_c$  approximated by a parabolic function (Kokusho et al. 2013).

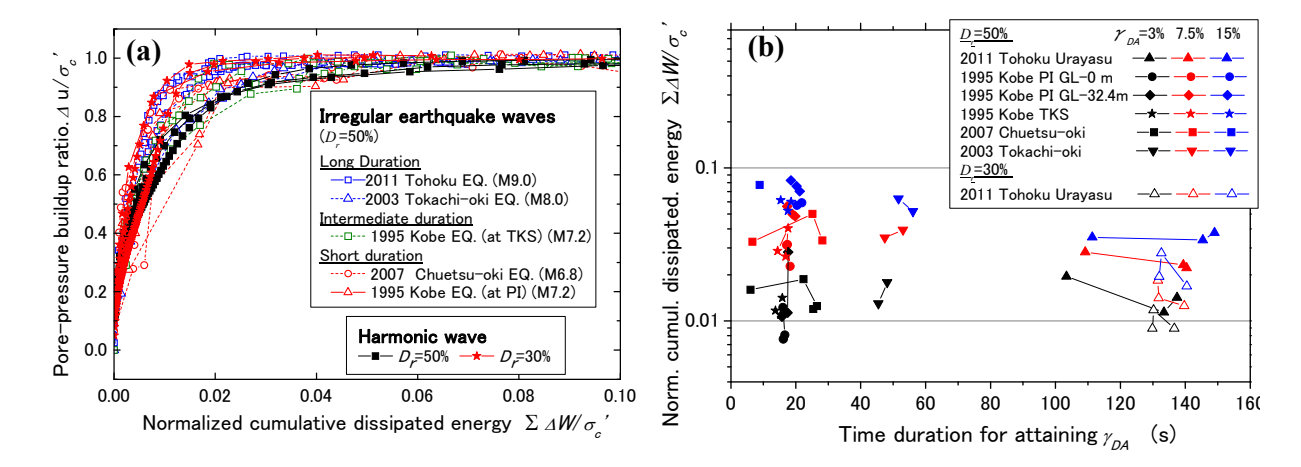


Figure 10. Effects of irregularity of various earthquake motions investigated by torsional shear tests on clean sand: (a) Pore-pressure buildup ratio versus cumulative dissipated energy, (b) Normalized cumulative dissipated energy versus time duration for attaining given induced strains (Kaneko 2015).

ent relative densities and fines contents and approximated by the following parabolic function for  $CRR \ge 0.1$  with the determination coefficient  $R^2$ =0.86.

$$\sum \Delta W / \sigma_c' = 0.032 - 0.48 \cdot CRR + 2.40 \cdot CRR^2$$
 [17]

This relationship between CRR and corresponding dissipated energy  $\sum \Delta W/\sigma_c$  in Figure 9 holds uniquely for sands with various densities and fines content for the present database on reconstituted sands at least. It is assumed here to be also applicable to natural sands with different soil fabric such as those formed in long geological histories. It is because the effect of soil fabric may possibly affect both CRR and  $\sum \Delta W/\sigma_c$  in such a way that the correlation will not differ considerably, though further test data is needed to demonstrate it. Based on the assumption, CRR versus  $N_1$  correlations, already established and used in SBM, may easily be transformed into  $\sum \Delta W/\sigma_c$  versus  $N_1$  correlations to be used in EBM.

#### 3.2 Test results by irregular motions

As for the irregularity of seismic waves, Figure 10(a) shows the normalized cumulative dissipated energies  $\sum \Delta W/\sigma_c$ ' plotted cycle by cycle versus corresponding pore-pressure ratio  $\Delta u/\sigma_c$ ' obtained by torsional simple shear tests on clean sand of  $D_c$ -50% using different types of recorded earthquake waves of various durations; the longest durations of more than 150 seconds (the Urayasu motion during 2011 Tohoku earthquake of  $M_J$ =9.0) to the shortest durations of 20 seconds (the Port Island motion during the 1995 Kobe earthquake of  $M_J$ =7.2). Also superposed are the plots obtained by the same tests on clean sands of  $D_c$ =50% and 30% conducted by harmonic

waves. Despite some data dispersions, almost all the  $\sum \Delta W/\sigma_c' \sim \Delta u/\sigma_c'$  curves for the irregular motions for  $D_r \approx 50\%$  are located in between the curves of  $D_r \approx 50\%$  and 30% by the harmonic wave. The difference depending of the different seismic waves are really trivial, though longer duration waves tend to attain slightly higher pressure ratios than shorter ones for the same dissipated energy.

In the vertical axis of Figure 10(b), the normalized cumulative dissipated energies obtained by the same torsional simple shear tests for attaining given induced strains  $\gamma_{DA}$  =3, 7.5, 15% are plotted. The horizontal axis stands for time durations needed to attain those strains from the start of irregular loading; namely the time duration tends to be shorter with increasing wave amplitudes even for the same seismic motion. Despite the local data fluctuations, the energy for individual  $\gamma_{DA}$  -values in the vertical axis are essentially distributed horizontally, independent of time for widely varying time durations from only 20 seconds (the 1995 Kobe earthquake) to 140 seconds (the 2011 Tohoku earthquake). This indicates that only the dissipated energy determines the induced strain during irregular loading, as in the harmonic motion, irrespective of wave amplitudes, durations, wave forms, etc.

#### 4. HOW TO COMPARE DEMAND WITH CAPACITY

In EBM by Kokusho (2013), the energy capacity for liquefaction is directly compared with the energy demand for a given earthquake motion in liquefiable surface soil layers. Upward SH-wave energy is considered here as the energy demand, because the wave energy causing liquefaction is the cumulative value and the associated downward energy also contributing the liquefaction constitutes a part of the upward energy originally. Some considerations needed to compare the energy capacity with the upward energy are discussed in the following.

#### 4.1 Dissipated energy in wave propagation

Let us consider the wave energy in the SH-wave propagating in a viscoelastic medium upward in the vertical z-direction as illustrated in Figure 11(a). The wave displacement is expressed using a sine function as:

$$u = Be^{-(\omega D/V_S)z} \sin \omega (t - z/V_S)$$
 [18]

and the particle velocity  $\dot{u} = du/dt$  becomes

$$\dot{u} = \omega B e^{-(\omega D/V_S)z} \cos \omega (t - z/V_S)$$
 [19]

Here,  $\omega$  =angular frequency, D=damping ratio, and B=displacement amplitude. According to Eq. 19, the energy of the SH-wave in one-wave length  $\lambda = V_s/f = 2\pi V_s/\omega$  passing through a unit horizontal area at z during the time from zero to one period  $T = 1/f = 2\pi/\omega$  is calculated as:

$$E = \rho V_{\rm s} \int_0^{1/f} (\dot{u})^2 dt = \pi \rho V_{\rm s} \omega B^2 e^{-2\beta z}$$
 [20]

From Eq. 20, the velocity amplitude  $\dot{u}_a$  and strain amplitude  $\gamma_a$  of the harmonic wave at z are correlated as:

$$\dot{u}_{a} = \left[\omega B e^{-(\omega D/V_{S})z} \cos \omega (t - z/V_{S})\right]_{\text{max}}$$

$$= \omega B e^{-(\omega D/V_{S})z} = -V_{S} \gamma_{a}$$
[21]

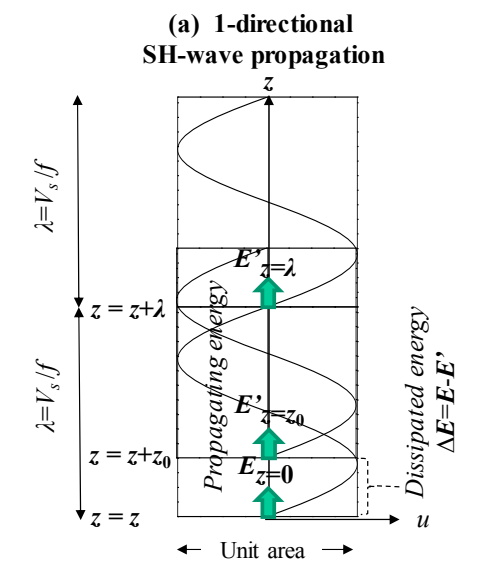
The energy E in Eq. 20 and the energy density per unit volume  $E/\lambda$  can be expressed using  $W=G{\gamma_a}^2/2$  defined by the triangular area illustrated in Figure 11(b) and also using Eq. 20 as follows.

$$E = \pi \rho V_{s} \omega B^{2} e^{-2(\omega D/V_{s})z} = \left[ \rho \left( \dot{u}_{a} \right)^{2} / 2 \right] \lambda = W \lambda$$
 [22]

$$E/\lambda = \rho (\dot{u}_a)^2 / 2 = G\gamma_a^2 / 2 = W$$
 [23]

Because E is the energy per unit area, it is correlated with W the energy per unit volume using the wave length  $\lambda$  as in Eqs, 22 and 23. The energy transported by harmonic waves is expressed as  $\rho \left(\dot{u}_a\right)^2 / 2$  or  $W = G \gamma_a^{\ \ 2} / 2$ , wherein the wave energy is shared evenly between the kinetic and strain energies.

The energy at  $z=z+z_0$ , E', shown in Figure 11(a) can be calculated using Eq.22 and written in a similar way as:



## (b) Cyclic loading of viscoelastic soil

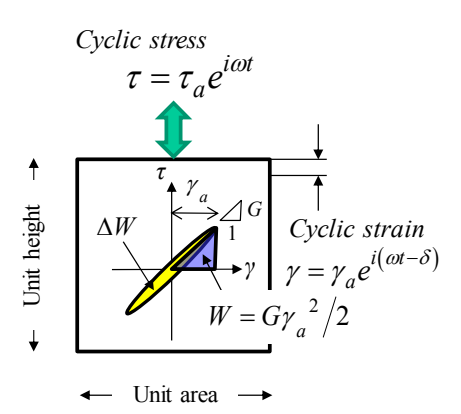


Figure 11: Comparison of wave energies *E* and *E'* in one-directional wave propagation (a), and associated stress-strain curve in cyclic loading test (b), in viscoelastic media.

$$E' = \pi \rho V_s \omega B^2 e^{-2(\omega D/V_s)(z+z_0)} = W e^{-2(\omega D/V_s)z_0} \lambda$$
 [24]

Then, the difference of wave energy in one wave length between E and E' is:

$$\Delta E = E - E' = \left(1 - e^{-2(\omega D/V_S)z_0}\right) W \lambda \tag{25}$$

Hence, the rate of the dissipated energy to the original wave energy is expressed using from Eqs. 22 and 25 as:

$$\Delta E/E = 1 - e^{-2(\omega D/V_S)z_0} = 1 - e^{-4\pi D(z_0/\lambda)}$$
 [26]

Hence, the dissipated energy ratio in one wave-length is written by putting  $z_0 = \lambda$  as:

$$\Delta E/E = 1 - e^{-4\pi D}$$
 [27]

If the damping ratio *D* is small enough,  $e^{-4\pi D} \approx 1 - 4\pi D$  using the Taylor series, Eq. 27 becomes:

$$\Delta E/E = 4\pi D$$
 [28]

The dissipated energy ratios  $\Delta E/E$  formulated in Eqs. 27

and 28 for one wave length are plotted versus the damping ratio D with thick solid lines in Figure 12(a). It is obviously seen that the two equations coincide at D=0 and tend to diverge with increasing D, because  $\Delta E/E$  in Eq. 27 approaches to unity, an upper limit for increasing D-values.

#### 4.2 Energy dissipation in cyclic loading

Eq. 28 has the same form as the dissipated energy ratio  $\Delta W/W = 4\pi D$  during cyclic loading in the viscoelastic material. This indicates that the ratio of dissipated energy for one wave length as illustrated in Figure 11(a) is determined by the same function of damping ratio D in cyclic loading shown in Figure 11(b), if the damping ratio D is small. Note that W is the maximum elastic strain energy in unit volume per a half cycle of loading, while  $\Delta W$  is the dissipated energy in one cycle. The reason why  $\Delta E/E$  is expressed by the same function of D as  $\Delta W/W$  is that the strain energy W in the first half cycle can be mostly recovered to be recycled in the second half cycle because the dissipated energy  $\Delta W$  is sufficiently small. This is what happens in the wave propagation, too, wherein the wave energy  $E = W\lambda$  passing through a unit area in one wave length  $\lambda$  is dissipated by  $\Delta E = \Delta W \lambda$ .

As the dissipated energy increases with increasing damping ratio D, it has to be compensated by the wave energy E in wave propagations or by the strain energy W in cyclic loading tests. In the stress-strain curve of the viscoelastic material illustrated in Figure 12(b), the strain energy provided in one-cyclic loading is Area (ABCD A'B'C'D'A), while the energy  $\Delta W = Area$  (ACDA'C'D'A) is dissipated in the specimen during the same cycle. Out of the one-cycle strain energy, the energy corresponding to Area(ABC) in the first 1/2 cycle can be recovered and recycled in the second 1/2 cycle for Area(A'B'C'). The

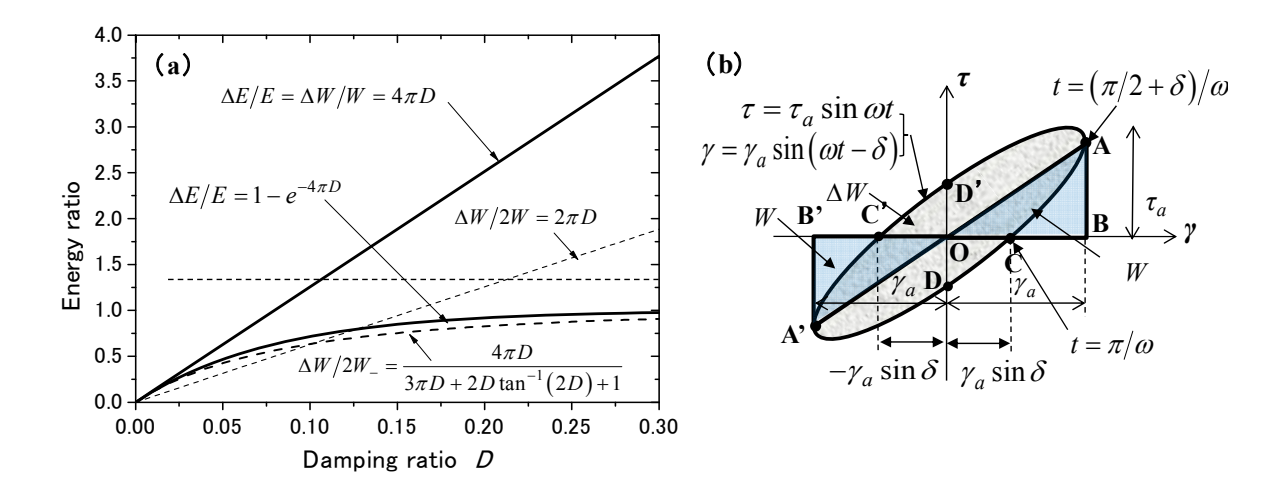


Figure 12.  $\Delta E/E \sim D$  curve in wave propagation compared with  $\Delta W/2W \sim D$  curve by cyclic loading (a), and Schematic stress-strain hysteresis loop of ideal viscoelastic material (b) (Kokusho 2016).

dissipated energy  $\Delta W$  is given as  $\Delta W = \tau_a \gamma_a \pi \sin \delta$  for the viscoelastic material (Ishihara 1996). By revisiting the same viscoelastic theory wherein shear stress  $\tau = \tau_a \sin \omega t$  is loaded to induce strain  $\gamma = \gamma_a \sin (\omega t - \delta)$  with a phase-delay angle  $\delta$ , the Area(ABC) is calculated by referring to Figure 12(b) as:

Area(ABC) = 
$$\omega \tau_a \gamma_a \int_{(\pi/2+\delta)/\omega}^{\pi/\omega} \sin \omega t \cos(\omega t - \delta) dt$$
  
=  $\Delta W \left[ 1 - 2(\pi/2 - \delta) D \right] / 4\pi D$  [29]

The energy denoted here as  $2W_{-}$  supplied in one cycle loading considering the energy recycling effect is thus obtained from  $\Delta W$  and Area(ABC) or Area(ABCD A'B'C'D') as:

$$2W_{-} = \left[\Delta W + Area\left(ABCDA'B'C'D'\right)\right]/2$$

$$= \left(\Delta W/4\pi D\right) \times \left\{3\pi D + 2D \tan^{-1}(2D) + 1\right\}$$
[30]

Then, the ratio of the dissipated energy  $\Delta W$  to the supplied energy  $2W_{-}$  is written as:

$$\Delta W/2W_{-} = 4\pi D/\{3\pi D + 2D \tan^{-1}(2D) + 1\}$$
 [31]

In Figure 12(a), the energy ratio  $\Delta W/2W_{-}$  in Eq. 31 versus damping ratio D is superposed with the dashed curve and compared with  $\Delta E/E = 1 - \mathrm{e}^{-4\pi D}$  in Eq.31. The two curves are very similar to each other, both have

almost the same initial tangent and tend to approach to the asymptote  $\Delta W/2W_- = \Delta E/E = 1.0$  with increasing D. This indicates that the energy dissipation mechanism during the wave propagation is very similar and almost reproducible in the cyclic loading. However, there is a small gap of maximum 10%, which may be attributed to the difference in loading: namely, simultaneous cyclic loading on a whole soil specimen versus time-delayed loading in situ accompanying wave attenuation during propagation.

In cyclic loading, the maximum elastic strain energy  $W=Area({\sf OAB})$  is normally employed to compare with the dissipated energy  $\Delta W$  as  $\Delta W/W=4\pi D$ . If the wave energy ratio  $\Delta E/E=1-e^{-4\pi D}$  is compared with energy ratios using  $\Delta W$  and W in Figure 12(a),  $\Delta E/E$  is more closely approximated by  $\Delta W/2W=2\pi D$  than  $\Delta W/W=4\pi D$  for D-value of 5% to 15% as indicated by the dotted line in the diagram. Nevertheless, it should be noted that the wave attenuation mechanism for larger D-value or larger internal damping during strong earthquakes can best be correlated with the cyclic loading mechanism by Eq. 31.

#### 4.3 Effect of free surface

There is an important issue about the energy demand for liquefaction that not all the upward energy is available in developing liquefaction in shallow ground. It was already stated above that the upward wave energy  $E_u$  is shared evenly by kinetic energy  $E_k$  and strain energy  $E_e$ , 50% each, both of which can supply the dissipated energy for liquefaction. However, if a stationary harmonic response of a soil column near free ground surface is considered for simplicity as illustrated in Figure 13, the stationary displacement vibration shown with the dashed curve with nodes and antinodes occurs due to the reflecting downward wave. Correspondingly, the strain energy  $E_e$  is zero at the surface or any other antinodes and 100% at the

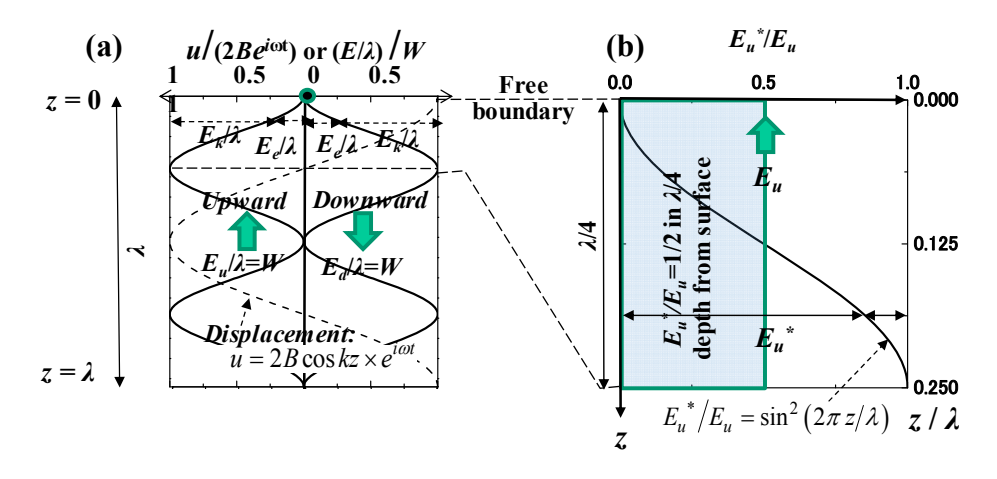


Figure 13. Wave energy versus depth near free ground surface: (a) Upward and reflected downward waves, (b) Upward wave energy in 1/4-wave length depth (Kokusho 2016).

nodes, while the kinetic energy  $E_k$  is vice versa as illustrated with the solid curves. Thus, the two kinds of energy are distributed with a fixed rate of 0 to 100% depending on the position and is not convertible to one another, quite different from the one-directionally propagating wave. This is, however, an extreme case in the steady-state harmonic motion of a particular frequency and may not represent a realistic seismic response by transient irregular short-duration motions, wherein nodes and antinodes are difficult to appear regularly along the depth. However again, the free ground surface consistently serves as an antinode of the displacement with zero strain energy for all frequencies and its effect cannot be ignored even in the irregular seismic motions. Consequently, it is postulated here that the surface boundary effect, though fading away with increasing depth, can reach down to 1/4 of the wave length  $\lambda = V_s T$  for a representative period of seismic motion T and the average wave velocity  $V_s$ , but not beyond that.

In Figure 13(b) the upward SH-wave in the shallow depth of  $\lambda/4$  from the surface is zoomed in. Considering the effect of the free surface boundary, the depth-dependent variation of the energy ratio for the harmonic wave with the representative wave length  $\lambda = V_s T$  may be formulated (Kokusho 2016) as:

$$E_{\mu}^{*}/E_{\mu} = \sin^2(2\pi z/\lambda)$$
 [32]

wherein  $E_u^*$  stands for the upward energy which can compensate dissipated energy, and  $E_u$  is the total upward energy at the same depth z. Namely, at the depth  $z=\lambda/4$ , the upward energy  $E_u$  consists of  $E_k$  50% and  $E_e$  50%, both of which can compensate the dissipated energy as in the one-directionally propagating wave energy ( $E_u^*/E_u=100\%$ ), while at the surface z=0,  $E_u$  is fixed to be composed of 100%  $E_k$  ( $E_u^*/E_u=0\%$ ) with no compensation for the dissipated energy allowed.

For earthquake motions, however, the applicability of Eq.32 is obviously unrealistic because of non-harmonic irregularity and nonlinear soil properties during strong earthquakes. Hence, the energy ratio in Eq.32 may well be simplified further and assumed as shaded in Figure 13(b) to take the average value 1/2 down to the depth of  $\lambda/4$  as:

$$E_u^*/E_u = 1/2$$
 [33]

Considering that dominant periods of earthquake motions T in most liquefiable site conditions may be T>0.5 ~ 1.0 s for average wave velocities  $V_s$ >160 m/s in surface soil deposits, the minimum depth of  $\lambda/4$  means around 20 m from the surface. This indicates that in normal liquefaction evaluation practice within the depth of 20 m, the up-

ward energy should be halved to compare with the liquefaction energy capacity.

#### 4.4 Capacity to be compared with demand

Another issue to consider in the present EBM is how to define the energy capacity to directly compare with the energy demand that is the upward energy. It was shown that the dissipated energy  $\Delta E$  relative to the wave energy *E* for SH-wave propagating is written as  $\Delta E/E = 1 - e^{-4\pi D}$ in Eq.27 using the damping ratio D. The dissipated energy  $\Delta E$  for liquefaction has to be supplied by the wave energy E in the field. It may well be assumed that the dissipated energy for liquefaction per unit wave length  $\Delta E/\lambda$ in in situ soil is identical to the dissipated energy density  $\Delta W$  for liquefaction measured in laboratory cyclic loading tests on the same soil. The maximum elastic strain energy density W is given in the half loading cycle, and the energy density  $\Delta W$  is dissipated in one cycle loading in an ideal viscoelastic material in Figure 12(b). As already mentioned, the in situ wave energy dissipation mechanism formulated as  $\Delta E/E = 1 - e^{-4\pi D}$  may be approximated by  $\Delta W/2W = 2\pi D$  for larger D-values associated with liquefaction behavior.

This observation in one-cycle loading may be extended to a similar relationship as:

$$\sum \Delta W / \sum 2W = 2\pi D$$
 [34]

for the cumulative energies  $\sum \Delta W$  and  $\sum 2W$  if damping ratio D can be represented by a constant value during cyclic loading liquefaction tests. A systematic test program actually shows that the damping ratio of sand is around D=0.1 to 0.2 with the average 0.15 during liquefaction tests as will be shown in Figure 14(b). Because the dissipated energy density for liquefaction  $\sum \Delta W$  is supposed to be identical both in situ and in the laboratory, the upward wave energy density should be compared in liquefaction potential evaluation with twice the cumulative elastic strain energy density  $\sum 2W$  which is correlated with the cumulative dissipated energy density  $\sum \Delta W$  in Eq.34. As stated above, the upward energy should be halved as Eq.33 to compare with the liquefaction energy capacity in the liquefiable shallow depth of 20 m. This means that  $\sum 2W$  correlated with dissipated energy density  $\sum \Delta W$ for liquefaction should be compare with the energy demand  $E_u^* = E_u/2$  instead of  $E_u$  per wave length  $\lambda$ . Because the upward wave energy  $E_u$  is defined here as the energy demand in the present EBM, the wave energy density  $E_u/\lambda$  should be compared with four times the cumulative maximum strain energy  $\sum 4W$ .

Apart from the ideal viscoelastic material, let us focus on actual soil behavior, now. Figure 14(a) exemplifies a

typical stress-strain relationship obtained in undrained cyclic loading triaxial tests on saturated sands. In Figure 14(b), the energy calculation results obtained from the stress-strain curves on the same sand are plotted cycle by cycle (Kokusho 2013). In the vertical axis, the elastic strain energy densities W ( $Area(ODD^c)$ ) multiplied by 4 because of the above-mentioned reason and summed up in the loading sequence as  $\sum W^* \equiv \sum 4W$  are plotted in the vertical axis with open symbols versus the cumulative dissipated energies  $\sum \Delta W$  (Area(ABCDEA)) in the horizontal axis. The same test data in Figure 7(b) is used here again in the plots, which may be approximated by the next equation to determine  $\sum W^*$  from the cumulative dissipated energy density for liquefaction  $\sum \Delta W$  (Kokusho 2013).

$$\sum W^* / \sigma_c' = 5.4 \times 10^{1.25 \times \log(\sum \Delta W / \sigma_c')}$$
 [35]

These  $\sum \Delta W \sim \sum W^*$  plots may be compared with the well-known formula  $\Delta W/W = 4\pi D$  using some representative values of D, in order to know if the damping ratio D can be represented by a constant value during cyclic loading liquefaction tests. The correlation  $\sum \Delta W/\sum W^* = \sum \Delta W/\sum 4W = \pi D$  for D=0.1, 0.15, 0.20 is shown with a set of dashed lines in Figure 14(b) to compare with the open symbol plots. Obviously, nearly all the plots for different relative density  $D_r$  and fines content  $F_c$  are in between D=0.10 and 0.20 throughout the cyclic loading tests and may be approximated by D≈0.15 as the average, confirming the assumption to draw  $\sum \Delta W/\sum 2W = 2\pi D$  in Eq.34 from  $\Delta W/2W = 2\pi D$ .

Apart from using the elastic strain energy W (Ar-ea(ODD') in a half cycle as in normal engineering practice, the strain energy actually needed in one cycle  $2W_{-}$  corresponds to Area (ABB'CDD'EA) minus Area (BB'C) in Figure 14(a) and can be evaluated in the same way as Eq. 29 as:

$$2W_{-} = \left[\Delta W + Area(ABB'CDD'EA)\right]/2$$
 [36]

In order to compare this with the cumulative dissipated energy in the same manner as  $\sum W^* \equiv \sum 4W$  versus  $\sum \Delta W$ ,  $2W_-$  is doubled here and summed up to individual cycles as  $\sum W_-^* \equiv \sum (2 \times 2W_-)$  and plotted versus  $\sum \Delta W$  with closed symbols in Figure 14(b) (Kokusho 2016). The relationship  $\sum W_-^* \sim \sum \Delta W$  is not so different from  $\sum W^* \sim \sum \Delta W$  for  $\sum \Delta W$  up to  $0.02 \sim 0.04$ , which corresponds to the threshold dissipated energy for initial liquefaction (Kokusho 2013). Beyond that energy,  $\sum W_-^*$  obviously gives higher energy than  $\sum W_-^*$ , while  $\sum W_-^*$  tends to be almost proportional to  $\sum \Delta W$  all the way from zero to 0.12. It is approximated by the next equation with a high coefficient of determination  $R^2$ =0.997.

$$\sum W_{-}^{*}/\sigma_{c}' = 2.06 \times \sum \Delta W/\sigma_{c}'$$
 [37]

The difference between Eqs.35 and 37 is partially attributed to that twice the elastic strain energy 2W given to a soil specimen in one cycle is correlated with  $\Delta W$  in the former while recycling of a part of the strain energy from

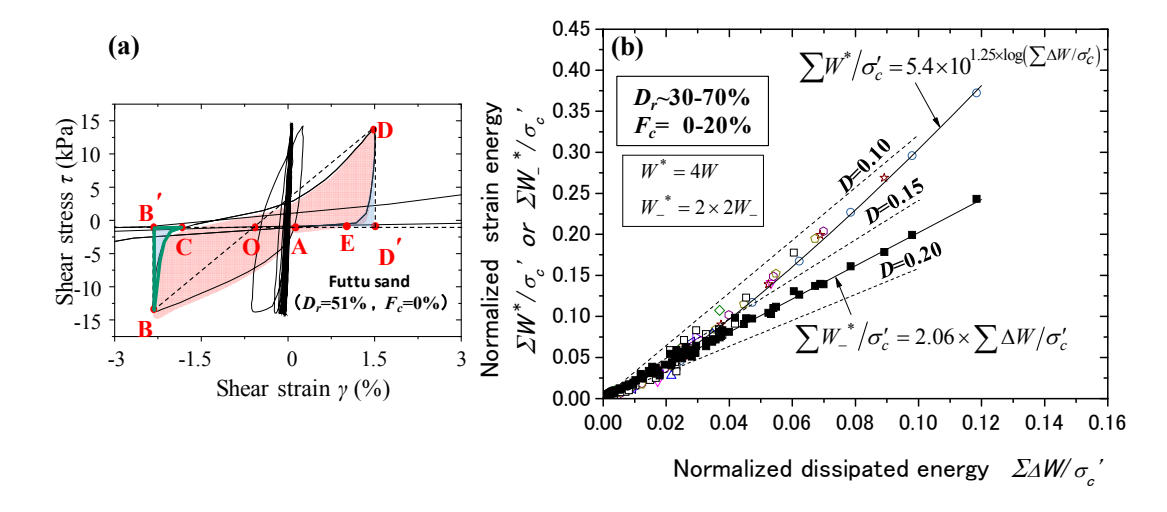


Figure 14. Typical stress-strain relationship in undrained cyclic loading triaxial test (a), and Energy calculation results obtained from a series of tests (b), (Kokusho 2016).

the first to the second half cycle loading is considered in the latter. The effect of nonlinear stress-strain curve on the calculated strain energy, the cyclic mobility effect in particular, may be another cause of the difference. If the notation  $\sum W_{-}^{*} \equiv \sum (2\times 2W_{-})$  is reminded here, Eq.37 implies  $\sum W_{-}^{*}/2 = \sum 2W_{-} = 1.03\times \sum \Delta W \approx \sum \Delta W$ . This allows a very simple interpretation that the cumulative dissipated energy  $\sum \Delta W$  is almost equal to the cumulative strain energy  $\sum 2W_{-}$  in Eq.36 actually supplied all through the liquefaction process. Thus, in the present EBM, the energy demand that is the upward energy is to be directly compared with the energy capacity defined as the cumulative strain energy density,  $\sum W_{-}^{*}$  in Eq.35 or  $\sum W_{-}^{*}$  in Eq.37, times the soil layer unit thickness to evaluate the liquefaction potential.

#### 5. EBM PROCEDURES

The evaluation steps for the EBM are illustrated in Figure 15 and explained below. Hereafter, the notation of summation  $\Sigma$  in terms of loading cycles will be abbreviated for simplicity, so that  $\sum\!\Delta W\,\to\,\Delta W$  and  $\sum\!W^*\,\to\,W^*$ .

- a) At a given site, a soil profile is divided into "soil units" of a constant thickness H=1 or 2 m in accordance with penetration test data with sequential numbers  $i=1\sim n$ . The normalized dissipated energy  $\Delta W/\sigma_c'$  for liquefaction is determined for each soil unit from penetration test results, using the  $CRR\sim N_1$  correlations in the SBM formulas combined with Eq.17.
- b) The normalized strain energy density  $W^*/\sigma_c'$  corresponding to  $\Delta W/\sigma_c'$  for liquefaction is evaluated by

- Eq.35, though Eq. 37 might also be used if  $W_{-}^{*}$  is employed as the strain energy density in place of  $W^{*}$ .
- c) Then the strain energy WH for the soil unit with the thickness H to liquefy is calculated as the energy capacity of the unit. In calculating  $W^*$  from  $W^*/\sigma_c'$ , the effective confining stress  $\sigma_c'$  is determined from the effective overburden stress  $\sigma_v'$  as  $\sigma_c' = (1 + 2K_0)\sigma_v'/3$ .
- d) The upward energy  $E_u$  is calculated here in Eq. 4 using a one-dimensional response analysis of the soil model to compare with the corresponding SBM results, and the ultimate energy at the end of shaking of a given earthquake motion  $E_{uf}$  is determined for each unit as the energy demand.
- e) The liquefaction energy capacity  $W^*H$  in each soil unit is directly compared with the energy demand  $E_{uf}$  by calculating an energy ratio  $W^*H/E_{uf}$ . A soil unit with a smaller value of the energy ratio  $W^*H/E_{uf}$  has higher and earlier liquefaction potential than other units in the same soil profile, although the overall liquefaction potential will be decided in g) below.
- f) The energy ratios of individual soil units over the soil profile are arranged and numbered in sequence starting from the lowest ratio (j=1) toward higher ones and summed up as  $\sum_{j} \left( W^* H / E_{uf} \right)_{j}$  following that sequence j, denoted here as AER (accumulated energy ratio).
- g) Liquefaction is considered to occur at most in those units where  $AER = \sum_{j} (W^*H/E_{uf})_{j} < 1.0$ , because the upward energy can liquefy individual soil units in the above-mentioned sequence until it is all consumed by the dissipated energies of those units.

Thus, in the present EBM, the energy demand  $E_{uf}$  is explicitly given, and liquefaction behavior is judged only in

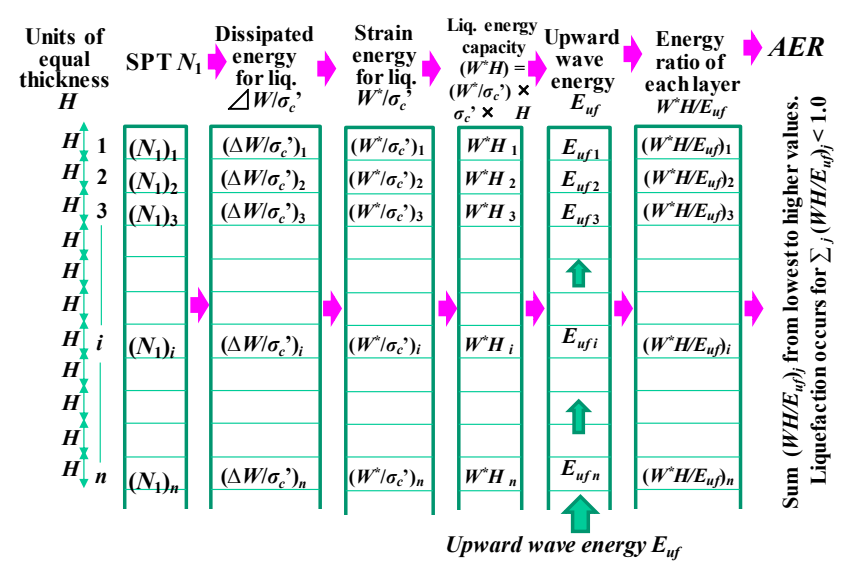


Figure 15: Evaluation steps in present EBM where energy demand is directly compared with energy capacity

those layers where their total energy capacities  $\sum_j (W^*H)_j$  corresponding to given induced strains are within the energy demand.

#### 6. TYPICAL EBM RESULTS COMPARED WITH SBM

#### 6.1 Uniform soil model

In order to compare the present EBM with SBM generally, the first soil model addressed here is a hypothetical uniform sand deposit 10 m thick underlain by a stiff base shown in Figure 16 (Kokusho 2013). The sand deposit  $K_0$ -consolidated with its normalized SPT N-value  $N_1$ =8,

effective overburden stress  $\sigma'_{v}$  and S-wave velocity  $V_{s}$  shown is divided into 5 layer units of H=2 m thick each (L1 to L5), wherein L1 is unsaturated (the density  $\rho_{t}$  =1.8 t/m³) and L2 to L5 are saturated ( $\rho_{sat}$  =1.9 t/m³).

A horizontal acceleration motion (K-NET Urayasu EW) during 2011 Tohoku earthquake (M=9.0) is given at the ground surface either in the real time scale (RT: duration 236 s) or in a compressed half time scale (RT/2: duration 118 s). In Figure 17, the two time histories (a) RT and (b) RT/2 given are shown at the top together with upward energies calculated in the individual units at the bottom. Note that the upward energy dramatically decreases down to about 1/8 if the time scale is halved (RT/2).

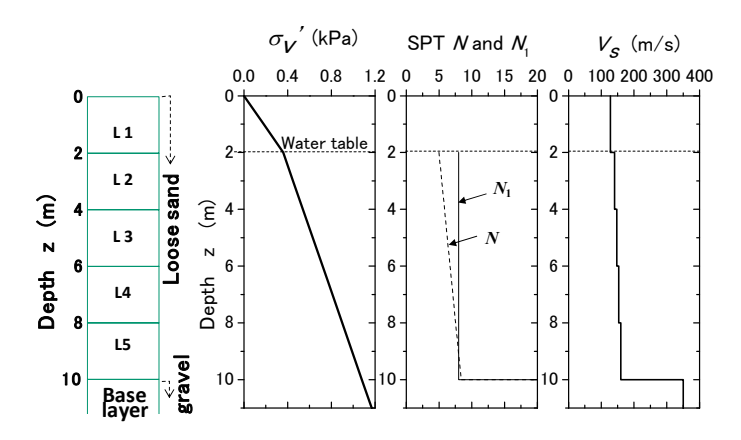


Figure 16. Uniform soil model for liquefaction evaluated by EBM and SBM (Kokusho 2013).

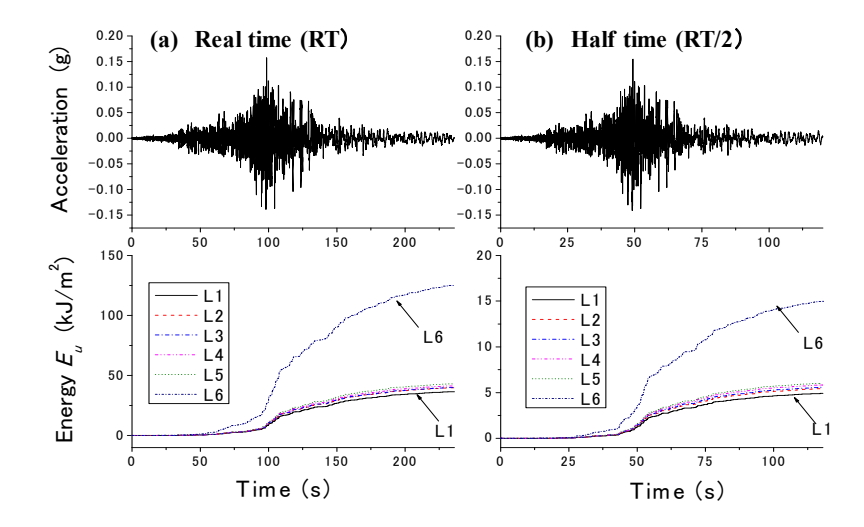


Figure 17: Time histories of acceleration (top) and upward wave energy (bottom) given to the soil model: (a) Real-time motion (RT), (b) Compressed half-time motion (RT/2) (Kokusho 2013).

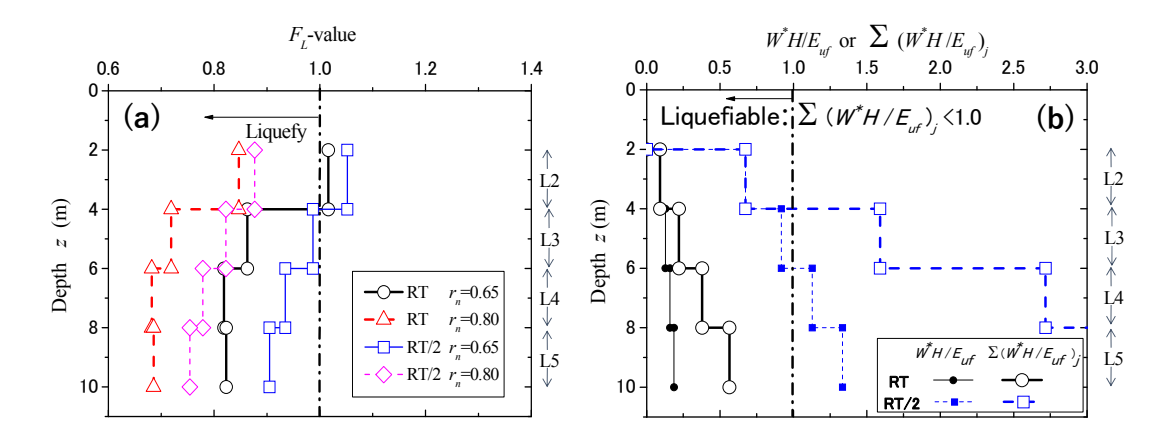


Figure 18: Liquefaction evaluation results by EBM and SBM for RT and RT/2 motions: (a)  $F_L$ -value versus depth, (b)  $WH/E_{uf}$  or  $\Sigma(WH/E_{uf})_i$  versus depth (Kokusho 2013).

In the SBM evaluation, the cyclic stress ratio is obtained from the maximum seismic shear stress  $\tau_{\rm max}$  and effective overburden stress  $\sigma'_{\rm v}$  as  $CSR = r_n \tau_{\rm max}/\sigma'_{\rm v}$ . Here, the stress reduction coefficient  $r_n = \tau_{\rm eq}/\tau_{\rm max} = 0.1(M-1)$  correlating equivalent harmonic shear stress amplitude  $\tau_{\rm eq}$  to maximum seismic shear stress  $\tau_{\rm max}$  (Tokimatsu & Yoshimi 1983) can be determined as  $r_n = 0.80$  for the M=9.0 earthquake and also  $r_n = 0.65$  for the default value. In Figure 18(a), the  $F_L$ -value thus evaluated is illustrated along the depth for the RT and RT/2-motions. The choice of  $r_n=0.65$  or  $r_n=0.80$  tends to have a greater effect on the  $F_L$ -value than the difference of input motions, RT or RT/2, indicating the importance of proper choice of  $r_n$  depending on the earthquake magnitude in SBM.

In the EBM evaluation, the normalized dissipated energy per unit volume to liquefy the sand layer of  $N_1$ =8 can be calculated from the SBM formula (JRA 2002) combined with Eq.17 as  $\Delta W/\sigma_c'$  =0.0281. Then, the corresponding strain energy per unit volume for liquefaction is given as  $W^*/\sigma_c' = 0.0621$  from Eq.35. The liquefaction energy capacities  $W^*H$  for the units H=2 m thick to liquefy are calculated using the corresponding average confining stresses  $\sigma'_c = \sigma'_v (1 + 2K_0)/3$ , with  $K_0$  =0.5. In Figure 18(b), the energy ratio  $W^*H/E_{uf}$  calculated in the individual units is shown along the depth with thin lines plus small solid symbols. Because the energy ratio W\*H/E<sub>uf</sub> is obviously smaller for the units in shallower depths both for RT and RT/2 motions, liquefaction tends to occur first in L2 and descend in sequence to the deeper units. The thick lines with large open symbols in the same figure are the values  $AER = \sum_{i} (W^*H/E_{uf})$  calculated in the EBM step (f) explained above. For the RT-motion shown by the thick solid lines, AER<1.0 for the summation from L2 to L5, indicating that the upward energy is enough to liquefy all the saturated units. In contrast, for the RT/2-motion shown by thick dashed lines, *AER*<1.0 only for L2, indicating that the upward energy is not enough to liquefy all but the unit L2. Thus, there exists a clear difference in liquefaction potential between the two input motions, reflecting the tremendous energy reduction in the RT/2-motion.

The results by EBM in Figure 18(b) can be compared with those by SBM in Figure 18(a). The results by SBM and EBM appear to be essentially consistent for the RT-motion in that all the saturated units are to liquefy. This consistency gets better if the stress reduction coefficient in SBM is chosen as  $r_n$  =0.80 considering the M=9.0 earthquake, while the effect of input motions is intrinsically included in EBM. However, the two results become considerably different in the RT/2-motion. The effect of the half-time scale is far more evident in EBM than in SBM because the former directly reflects the energy reduced to 1/8. Another qualitative difference between the two methods is that the liquefaction potential is higher in the shallower units than in the deeper units in the uniform sand deposit in EBM, whereas it is vice versa in SBM.

#### 6.2 Liquefaction case by far-field earthquake

The next is a case history on a filled farmland which lique-fied and fluidized during the 2003 Tokachi-oki earthquake (M=8.0) in Hokkaido, Japan. The site was 230 km far from the epicenter of the plate-boundary earthquake, and the maximum acceleration recorded nearby was only 0.05 g as indicated in the acceleration time history in Figure 19(a). An area, 200 m long and 50 m wide, subsided by 3.5 m maximum and boiled sand erupting from two ejection holes flowed 1 km downstream along a ditch. The soil models with each unit thickness H=1 m were developed consisting of the L1~L7 units where the upward energies were calculated as shown in (b), and the depth-

dependent SPT *N*-values for individual units were determined from SWS sounding data at eight investigation points as shown in Figure 19(c) using an empirical formula developed in Japan (Inada 1960). The thickness of the soft sandy fill was variable (4~7 m) depending on the SWS investigation points and the water table was 1~2 m below the ground surface (Tsukamoto et al. 2009). The normalized dissipated energy densities  $\Delta W/\sigma_c'$  in individual units were evaluated from the *N*-values in the same manner as mentioned in the uniform model but considering the average fines content ( $F_c$ =33%) in the design code (JRA 2002). The seismic shear stress  $\tau_{\rm max}$  and upward energy  $E_u$  was calculated using the 1D response analysis with the input motion, K-NET Kitami in Figure 19(a), given at the surface.

In Figure 20(a), liquefaction potentials evaluated by EBM ( $AER = \sum_j \left(W^*H/E_{uf}\right)_j$ ) for individual depths are plotted with close symbols connected with solid line at two representative soil investigation points, P1 and P7. Because AER <1.0 is the condition for liquefaction, the shallower portion will liquefy both at P1 and P7 according to this EBM.

By the way, a significant simplification by Eq.33 is employed in the present EBM so that the upward energy  $E_u^*$  to be able to compensate the dissipated energy is constant as  $E_u^*/E_u=1/2$  within the depth of a quarter wave length from the ground surface (named here as Method-A). However, there may be more or less a certain depth-dependency of the energy ratio  $E_u^*/E_u$ , actually. Hence, a comparative study has been conducted to take into ac-

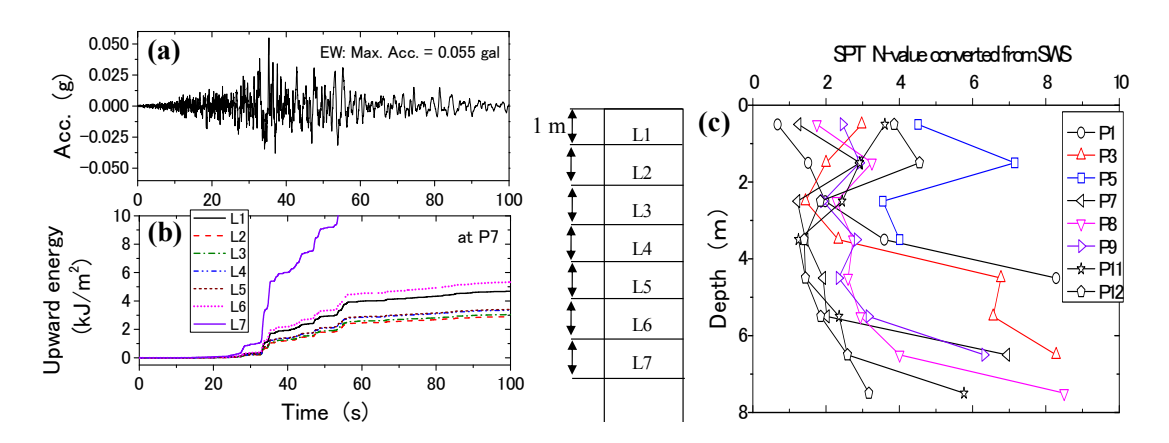


Figure 19: Acceleration time history given to fill farm land liquefied during a far-field *M*8.0 earthquake with max. acc. about 0.05 g (a), Associated upward energies (b), and SWS-converted N-values versus soil depths at investigation points in liquefied site (c) (Kokusho and Mimori 2015).

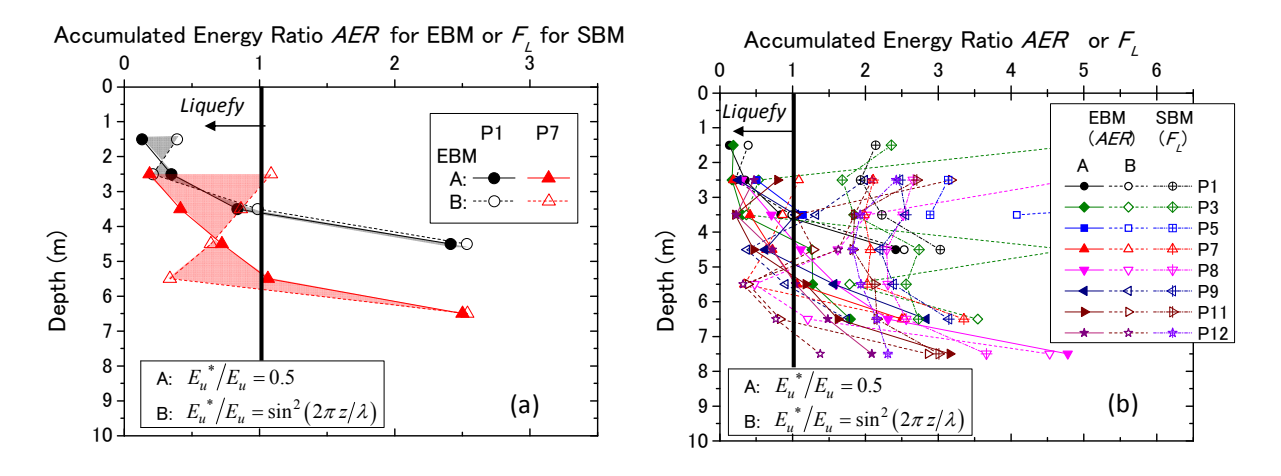


Figure 20: AER-values by for Method-A and B in EBM plotted versus soil depth: (a) At P1 and P7, (b) At eight investigation points and compared with  $F_L$ -values by SBM (Kokusho 2016).

count the depth-dependent variation of  $E_u^*$ , wherein  $E_{\mu}^{*}/E_{\mu} = \sin^{2}(2\pi z/\lambda) = \sin^{2}(2\pi t/T)$  in Eq.32 is used (named as Method-B) in place of Eq.33 to consider the extreme depth-dependent effect. Here, t is the travel time of the SH wave from the ground surface to a particular depth z using strain-dependent degraded S-wave velocities in individual layers, T is the dominant period of seismic motion, and otherwise the same EBM procedure is followed here (Kokusho 2016). In Figure 20(a), the AERvalues obtained by Method-B (open symbols connected w ith dashed lines) are superposed at two representative points P1 and P7 to compare with those by Method-A. Though the liquefied depths tend to be deeper in Method-B than in A, the difference is not so significant. The liquefaction may most probably occur in the shaded area on the diagram in between the two lines of Method-A and B, because they seem to represent the two most extreme cases. In Figure 20(b) the same results for all eight points are shown for EBM and SBM. Again, all the points except P5 are evaluated liquefiable also in Method-B as in Method-A. In a clear contrast, the SBM-evaluation results superposed on the same diagram indicates no possibility of liquefaction at all because  $F_L$ -values are well above 1.0 despite that the effect of the earthquake magnitude M8 is taken into account by choosing the stress reduction coefficient  $r_n$  =0.70. In EBM, Method-A may well be recommended as a simplified and practical tool on a safer side in evaluating liquefaction potential in shallow depths (Kokusho 2016).

Thus, the EBM can predict liquefaction behavior very simply just by comparing the energy demand (upward energy) with the energy capacity (directly correlated with the dissipated energy for liquefaction by Eq.35 or 37). It may be able to readily take account of various aspects of input seismic motions (dominant period, duration, number of wave cycles and irregularity) only in terms of energy, and hence can be of a great help to examine the reliability of conventional SBM liquefaction evaluations for a variety of earthquakes motions. It is still necessary, however, to apply this EBM to more case histories to demonstrate its reliability in much more practical conditions.

#### 7. SUMMARY

The proposed Energy-Based Method (EBM) for liquefaction evaluation has been characterized in this paper in several respects, and compared with the Stress-Based Method (SBM) in some examples, yielding the following major conclusions.

 In the present EBM, the upward seismic wave energy as the energy demand is directly compared with the energy capacity of a liquefiable layer. This method has a great advantage in that the energy demand for liquefaction can automatically reflect the effects of earthquake durations, dominant periods and wave forms. The energy capacity or dissipated energy almost

- uniquely determines the pore-pressure build-up and induced strains in soil deposits. Thus, this method is completely free from the difference in seismic wave parameters such as amplitude, frequency components, duration and wave forms.
- 2) The upward energy  $E_u$  can be evaluated directly from acceleration motions to be used in SBM by one-dimensional soil response analyses. More simply, it can be estimated from the incident wave energy at a base layer and the impedance ratio between the sloping layer to the base layer based on empirical formulas derived from a number of vertical array records. The base incident energy may be reasonably estimated from earthquake magnitude and source to site distance by empirical formulas for engineering purposes.
- 3) The dissipated energy density accumulated to a given cycle, ∆W, is almost uniquely correlated with pore-pressure buildup and induced axial strain for each relative density. The ∆W -value thus evaluated is quite insensitive to the number of load cycles N<sub>c</sub> to induce a given strain under different cyclic stress ratio R<sub>L</sub>, indicating that the R<sub>L</sub>~N<sub>c</sub> correlation used in the stress-based method (SBM) can be interpreted as an equal-dissipated energy line. The irregularity of earthquake motions have only insignificant impacts on these correlations, indicating that the dissipated energy determines the soil liquefaction behavior almost uniquely.
- 4) In order to compare the upward energy  $E_u$  as the energy demand directly with the energy capacity, it is necessary to correlate cumulative dissipated energy  $\Delta W$  for liquefaction with strain energy  $W^*$  by Eq.35, or more precisely with  $W_-^*$  by Eq. 37, based on laboratory cyclic loading tests (the summation signs for cyclic loadings are abbreviated here). Because of the free surface condition, it is also necessary to introduce the simplification that the upward energy to be compared with the energy capacity should be reduced to 1/2 within the depth of 20 m.
- 5) With regard to the near-surface upward energy reduction by 1/2, EBM assuming a more drastic near-surface energy reduction for the harmonic motion having a dominant period of the earthquake motion can still predict the liquefaction at similar depths in the liquefaction case study during a far-field M8.0 earthquake in contrast to SBM which cannot. Thus this simplification seems to be adequate because it gives a safer side as a practical evaluation.
- 6) Thus, liquefaction case studies have demonstrated that, for a normal ground motion, EBM tends to give basically compatible results with SBM. However, disparities appear between them for ground motions with small peak accelerations and high energy or high accelerations and low energy, probably because the coefficient rn cannot be properly chosen in SBM for those cases. Considering that the dissipated energy controls the liquefaction mechanism according to many laboratory soil tests it seems reasonable to employ EBM as a comparable review tool for SBM in cases where engineers cannot be confident for various ground motions.

#### 8. REFERENCES

- Davis R.O., Berrill, J. B. 1982. Energy dissipation and seismic liquefaction of sands. *Earthquake Engineering and Structural Dynamics*, Elsevier, No. 10, 59–68.
- Figueroa, J. L., Saada, A. S., Liang, L. and Dahisaria, N. M. 1994. Evaluation of soil liquefaction by energy principles, *Journal of Geotechnical Engineering*, ASCE, 120 (9), 1554-1569.
- Inada, T. 1960. On the use of Swedish weight sounding test results, Tsuchi-to-Klso, Journal of Japanese Geotechnical Society, Vol.8, No.1, 13-18, in Japanese.
- Ishihara, K. 1996. Soil behaviour in earthquake geotechnics, Chapter 3, Oxford Science Publications, 16-39.
- JRA (Japan Road Association). 2002. Liquefaction potential evaluation method, *Design code for road bridges; Seismic design*, Maruzen Publishing Co. Ltd., 65-66 (in Japanese).
- Kaneko, Y. 2015. Energy based analysis of liquefaction using hollow cylinder tests -Influence of irregular loading and confining pressure-, *Master's Thesis (in Japanese)*, Graduate School of Science & Engineering, Chuo University, Tokyo, Japan.
- Kazama, M., Suzuki, T. and Yanagisawa, E. 1999. Evaluation of dissipated energy accumulated in surface ground and its application to liquefaction prediction, *Journal of Japan Society for Civil Engineers* (in Japanese), JSCE, No. 631/III-48, 161-177.
- Kokusho, T. and Motoyama, R. 2002. Energy dissipation in surface layer due to vertically propagating SH wave, *Journal of Geotechnical and Geoenvironmental Engineering*, ASCE, Vol.128, No.4, pp. 309-318.
- Kokusho, T. and Suzuki, T. 2011. Energy flow in shallow depth based on vertical array records during recent strong earthquakes, Soil Dynamics & Earthquake Engineering, Vol. 31, 1540-1550.
- Kokusho, T. and Suzuki, T. 2012. Energy flow in shallow depth based on vertical array records during recent strong earthquakes(Supplement), Soil Dynamics & Earthquake Engineering, Vol. 42, 138-142.
- Kokusho, T. 2013. Liquefaction potential evaluation energy-based method versus stress-based method-, Canadian Geotechnical Journal No. 50, 1-12.
- Kokusho, T., and Mimori, Y. 2015. Liquefaction potential evaluations by energy-based method and stressbased method for various ground motions, Soil Dynamics & Earthquake Engineering, Elsevier, Vol. 75, 130–146.
- Kokusho, T. 2016. Applicability of energy-based liquefaction potential evaluation method compared with FL-method –Supplement-, Geotechnical Journal (in Japanese), Japanese Geotechnical Society, 11 (3)283-293.
- Nemat-Nasser, S. and Shokooh, A. 1979. A unified approach to densification and liquefaction of cohesionless sand in cyclic shearing, Canadian Geotechnical Journal, 16, 659-678.
- Sarma, S. K. 1971. Energy Flux of Strong Earthquakes, Techtonophysics, Elsevier Publishing Company, 159-173

- Schnabel, P. B., Lysmer, J. and Seed, H. B. 1972. SHAKE – A Computer Program for Earthquake Response Analysis of Horizontally Layered Sites, Report EERC 72-12, University of California, Berkeley.
- Timoshenko, S. and Goodier, J. N. 1951. *Theory of Elasticity*, McGraw-Hill.
- Towhata, I. and Ishihara, K. 1985. Shear work and pore water pressure in undrained shear, *Soils & Foundations*, Vol.25, No.3, 73-84.
- Tokimatsu, K. and Yoshimi, Y. 1983. Empirical correlation of soil liquefaction based on SPT N-value and fines content, *Soils and Foundations*, 23 (4), pp. 56-74.
- Tsukamoto, Y. Ishihara, K. Kokusho, T. Hara, T. Tsutsumi, Y. 2009. Fluidisation and subsidence of gently sloped farming fields reclaimed with volcanic soils during 2003 Tokachi-oki earthquake in Japan, *Earthquake Geotechnical Case Histories for performance-based Design*, pp. 109-118
- Yanagisawa, E. and Sugano, T. 1994. Undrained shear behaviors of sand in view of shear work, *Intern. Conf. on SMFE* (Special Volume on Performance of Ground and Soil Structures during Earthquakes), New Delhi, India, Balkema Publishers 155-158.